Supporting Information

Kath et al. 10.1073/pnas.1321076111

SI Experimental Procedures

Proteins and Buffers. *Escherichia coli* proteins were purified from overproducing strains as previously described and untagged unless otherwise noted: polymerase (Pol) IV (1) and Pol IV^{C} (ΔC5) (2); the Pol III holoenzyme subunits α, δ, and δ′ (3); ε and θ (4); the WT clamp β (5), N-terminally his$_6$- and heart muscle kinase-tagged β^{R} (E93K-L98K), and β^{+}/β^{C}, a stable dimer formed from N-terminally Myc-tagged β and his$_6$- and heart muscle kinase-tagged β(ΔC5) (6); and τ and refolded ψ within the χψ-complex (7). The Pol III αεθ core and clamp loader assembly with the stoichiometry $\tau_3\delta\delta'\chi\psi$ were each reconstituted and purified following reported protocols (7).

The quality of purified protein was determined by comparing the activities of multiple preparations. A fraction of inactive or misfolded polymerases, inevitable in purification, would either fail to bind the clamp and not be observed in synthesis or bind and result in termination events or extended pauses. Because our conclusions depend on the reduction of pause times because of polymerase exchange, they are unlikely to be affected by inactive protein. If the fractions of active protein in the Pol III and Pol IV preparations used differed, the molar ratio of active Pol IV to active Pol III would differ from the ratio determined by protein concentration (Fig. 5) by a constant factor throughout this work and similarly not affect our conclusions.

Synthesis of an N^2-furfuryl-dG–Containing Oligonucleotide. The 20-mer oligonucleotide containing the N^2-furfuryl-dG lesion was constructed as previously described (8). A 20-mer oligonucleotide containing a fluoro substituent at the N^2 position of guanine (**X**) was purchased from Chemgenes: 5′-CTA CCT **X**TG GAC GGC TGC GA-3′. A fraction of the product was found to contain a hydroxyl group in place of the fluorine, the result of NaOH treatment to separate the oligonucleotide from the resin during manufacture. The fluorine was displaced with a fufuryl group by treating the oligonucleotide with fufurylamine, leaving the contaminating N^2-hydroxyl-dG unaffected. Fufurylamine treatment was followed by HPLC and MALDI-TOF MS as described (8) to remove the hydroxyl-containing oligonucleotide to obtain a pure 20-mer with the N^2-fufuryl-dG lesion.

M13 ssDNA with a Site-Specific DNA Lesion. ssDNA with a site-specific DNA lesion was constructed using M13mp7(L2), a mutant phage that contains an EcoRI site within a stable hairpin in its genome (Fig. S1*B*). Phage stock was a gift from John Essigmann (Massachusetts Institute of Technology, Cambridge, MA). A protocol to purify phage genomes and ligate a lesion-containing oligonucleotide at the digested EcoRI site (9) was adapted for this study with the following modifications. After PEG precipitation, the isolated phage pellet was extracted two or three times with 25:24:1 phenol:chloroform:isoamyl alcohol and one time with pure chloroform. DNA in the final aqueous layer was ethanol-precipitated and redissolved in 10 mM Tris (pH 8.5) buffer to ∼2 μg μL^{-1}; 100 μg M13mp7(L2) DNA was linearized in a 100-μL digestion reaction with 40 U EcoRI-HF (New England Biolabs) and 1× Buffer 4 at 23 °C for 8 h and purified with sequential phenol:chloroform:isoamyl alcohol and chloroform extractions and an ethanol precipitation. Then, it was dissolved in 100 μL Tris buffer. Purification of linear ssDNA prevented degradation in later steps.

Thirty picomoles 5′-phosphorylated oligonucleotide insert 5′-CTA CCT **X**TG GAC GGC TGC GA-3′ (**X** = N^2-furfuryl-dG or the dG control) was ligated at 16 °C overnight into 20 pmol purified linear ssDNA using annealed scaffold oligonucleotides 5′-AAA ACG ACG GCC AGT GAA TTT CGC AGC CGT CC-3′ and 5′-GGT AGA CTG AAT CAT GGT CAT AGC-3′ (25 pmol each) and 800 U T4 DNA ligase (New England Biolabs) in a 60-μL reaction. To remove the scaffold oligonucleotides, unligated linear M13 DNA, and excess insert, the mixture was subsequently treated at 37 °C for 4 h with 18 U T4 DNA polymerase and 80 U exonuclease I (New England Biolabs). The DNA was finally purified by sequential phenol:chloroform:isoamyl alcohol and chloroform extractions, ethanol-precipitated, and dissolved in 50 μL 10 mM Tris buffer to obtain the lesion-containing (or control) phage ssDNA.

The progress of DNA construction was monitored by taking samples at each step and separating them on a 0.8% Tris-acetate-EDTA agarose gel stained with ethidium bromide (Fig. S5*C*). As a control to guarantee that EcoRI completely linearized the hairpin-containing M13mp7(L2) ssDNA, which if uncut, could contaminate lesion-containing DNA, a mock ligation reaction was performed with digested ssDNA and scaffolds but without the insert. The mock reaction was then treated with T4 DNA polymerase and Exo I, which together degrade linear but not circular ssDNA. Degradation was nearly complete, showing efficient digestion of the hairpin (Fig. S5*C*).

Single-Molecule DNA Substrates. Linear end-labeled single-molecule DNA substrates were constructed using circular 7.2-kb M13 phage genomes (Fig. S1*A*). Experiments on undamaged DNA used substrates generated from M13mp18 ssDNA (New England Biolabs). Sixteen microliters this DNA (250 ng μL^{-1}) was annealed in 20 μL with 1 μM oligonucleotide mp18-SalI (Table S1) by heating to 65 °C for 10 min and slowly cooling to room temperature. Ten microliters annealed DNA was linearized at the dsDNA region with 10 U SalI (New England Biolabs) and 1× Buffer 3 in 50 μL at 37 °C for 1 h. Forty microliters restriction digest reaction was mixed to a final volume of 55 μL with 30 nM end-labeled oligonucleotides M13-5′-biotin and phosphorylated M13-3′-dig and 30 nM scaffolding oligonucleotides mp18-scaffold-1 and mp18-scaffold-2 (Table S1). The scaffolds were annealed to the linearized phage DNA and the end-labeled oligonucleotides by heating to 65 °C for 20 min and cooling to room temperature, also inactivating SalI; scaffold-mediated ligation was subsequently performed overnight at 16 °C with 400 U DNA ligase (New England Biolabs). The reaction was stopped by heat-inactivating ligase at 65 °C for 10 min and adding EDTA (20 mM final) to the cooled mixture. The stock solution (final substrate concentration ∼ 5 nM) was stored at 4 °C.

Single-molecule DNA substrates containing a site-specific lesion (Fig. S1*B*) were prepared similarly from lesion-containing M13mp7(L2) DNA (see above). ssDNA containing the N^2-furfuryl-dG lesion or the control dG was annealed with mp7L2-AlwNI (Table S1) and digested with 20 U AlwNI (New England Biolabs) in 1× Buffer 4 at 37 °C for 1 h. Linearized DNA was ligated to M13-5′-biotin and phosphorylated M13-3′-dig using the scaffolding oligonucleotides mp7L2-scaffold-1 and mp7L2-scaffold-2 (Table S1).

The annealed oligonucleotide mp18-scaffold-1 (for the undamaged substrate) or mp7L2-scaffold-1 (for the lesion-containing substrate) near the 3′ terminus of the linear M13 template served as the primer for DNA synthesis. For the lesion-containing substrate, the primer terminus is situated ∼3,150 nt from the N^2-furfuryl-dG site.

Single-Molecule Flow Stretching Experiments. Single-molecule experiments were performed at 23 °C using custom microfluidic

flow cells with glass coverslips as described previously (10). In summary, primed end-labeled M13 bacteriophage ssDNA was attached to the glass surface of the flow cell by a biotin-streptavidin linkage on one end and a micrometer-scale bead (tosyl-activated, 2.8-μm diameter; Dynal) by a digoxigenin–antidigoxigenin interaction on the other end. A magnet exerts a weak force of ∼1 pN to lift the paramagnetic bead off the surface, and laminar flow of buffer through the flow cell exerts a constant force of ∼3 pN on the bead and by extension, uniformly throughout the DNA tether. At this low force, ssDNA is entropically coiled, whereas dsDNA is stretched to nearly its crystallographic length (Fig. S1*C*). Conversion of ssDNA to dsDNA during primer extension can, therefore, be observed and tracked by extension of the DNA tether and movement of the coupled bead.

Glass coverslips were functionalized with a ratio of biotinylated PEG succinimidyl valerate:methyl-PEG succinimidyl valerate (Laysan Bio) of 0.75%:15% (wt/vol) in 0.1 M $NaHCO_3$ (pH 8.2) (10). Dried coverslips, stored under vacuum, were stable for several months.

Before an experiment, the functionalized coverslip surface was incubated with 0.2 mg mL^{-1} streptavidin (Sigma) in PBS for 30 min and then washed and incubated with blocking buffer (20 mM Tris·HCl, pH 7.5, 50 mM NaCl, 2 mM EDTA, 0.2 mg mL^{-1} BSA, 0.005% Tween 20) for an additional 30 min; 2–4 μL M13 substrate stock (∼5 nM; see above) was diluted with 500 μL blocking buffer and drawn into the flow cell at 0.025 mL min^{-1} with a syringe pump (Harvard Apparatus 11 Plus), allowing binding of DNA by the 5′-biotinylated ends to immobilized streptavidin sites. A stock of α-digoxigenin–functionalized polystyrene beads (tosyl-activated, 2.8-μm diameter; Dynal) was prepared as previously described (10); 2 μL bead stock was diluted with 500 μL blocking buffer and drawn into the flow cell at 0.025 mL min^{-1} to specifically bind the 3′-digoxigenin–labeled DNA substrates. Excess beads and DNA were removed from the flow cell by washing with 1 mL blocking buffer (>100 volumes) at 0.035 mL min^{-1}.

Immediately before the synthesis reaction, ∼150 μL replication buffer was introduced to exchange buffer. A solution of 500 μL replication buffer with replication proteins and nucleotides was added at 0.015 mL min^{-1}. A magnet exerting a weak force of ∼1 pN was used to lift the tethered paramagnetic beads off the surface; laminar flow at this rate through the flow cell exerts a constant force of ∼3 pN on the tether. After 2 min to allow the flow to stabilize, several hundred beads were visualized using dark-field microscopy through a 10× objective (Olympus) and imaged with a QIClick CCD camera (Q-Imaging). Data were recorded for 2,750 frames at 2 Hz using the software package Micro-Manager (www.micro-manager.org).

Primer extension on each individual molecule was observed by the motion of its bead in the direction of flow as the entropically coiled ssDNA was converted to extended dsDNA as previously indicated. Synthesis was not observed when dNTPs were excluded.

Single-Molecule Data Analysis. Individual beads were fit to 2D Gaussians and tracked with high accuracy (σ ∼ 20 nm) using the software package DiaTrack (Semasopht); beads nonspecifically stuck to the surface were used to subtract drift uniformly from all trajectories. Raw data for bead displacement in nanometers were converted into the number of base pairs synthesized using a calibration factor of 3.9 bp nm^{-1} determined by dividing the substrate length (7,249 bp) by the differential extension of ssDNA and dsDNA at the flow rate used (1,848 nm) (Fig. S1*C*).

To confirm the calibration factor and show the ability to observe a site-specific block of replication in the single-molecule primer extension assay, the dideoxy chain-terminated oligonucleotide 5′-GCT AAC GAG CGT CTT TCC AGA GCC TAA TTT GCC AGT TA-ddC-3′ (Integrated DNA Technologies) was annealed onto the M13mp18 single-molecule substrate ∼3,000 bp from the primer terminus. Synthesis was performed with T7 DNA polymerase exo$^-$, a gift from Charles Richardson (Harvard Medical School, Boston); primer extension terminated at the expected location (Fig. S1*D*).

Single-molecule trajectories were selected where the tethered DNA length increased in the direction of flow (y) but not the transverse direction (x). Trajectories that had a rapid simultaneous jump in both x and y represented sticking or unsticking of the bead to the surface of the flow cell and were excluded from analysis.

Synthesis trajectories were fit to segmented lines, with each segment corresponding to a Pol III event, a Pol IV event, or a pause using custom MATLAB code (Mathworks). Initial estimates for boundaries between segments were selected manually. The middle 80% of each region was then fit to a line, and new segment boundaries were determined from the intersection between adjacent segments. The processivity and rate for a segment are defined as the rise and slope, respectively.

Statistically significant synthesis events were defined as having a processivity greater than 3σ of the trajectory's noise (determined for individual trajectories but generally ∼200 bp); events were otherwise defined as pauses. A cutoff of 45 bp s^{-1} was used to assign significant synthesis events to Pol III (faster) or Pol IV (slower). This cutoff captures 93% of Pol III events and 95% of Pol IV events in experiments with individual polymerases.

Single-molecule data were binned to generate distributions and normalized to integrated counts, generating probability densities to facilitate comparisons. Fits of normalized histograms to one-term exponentials of the form $A \times \exp(-x/\lambda)$ for processivities (Fig. 1 and Figs. S3 and S7*B*) and $A \times \exp(-t/\tau)$ for pauses (Fig. 4 and Figs. S2, S6, and S7*A*) were determined using the MATLAB command fit, which generated the exponential fit constant (τ or λ).

Statistical comparisons were made between full datasets with the two-tailed Wilcoxon rank sum test using the MATLAB function ranksum and a significance level of $P = 0.05$.

Comparisons of Pause and Exchange Data. The slow rate of Pol IV (10.8 bp s^{-1} on average) implies that it takes ∼3σ/(10 bp s^{-1}) or ∼20 s to distinguish a Pol IV event from a pause. This lower bound for detection leads to undersampling of pauses less than 20 s for experiments with Pol IV alone and introduces noise in the determination of Pol III and Pol IV exchange times; however, these times are not similarly undersampled, because exchange is observed as a change in polymerase rate. We, therefore, binned the times in Fig. 4*A* and Fig. S2 *D*–*G* by 20-s intervals and when fitting curves to these distributions, excluded the first bin.

For statistical comparisons between full datasets in Fig. 4 and Figs. S6 and S7*A*, the Bonferroni correction for multiple sample comparisons was used to determine significance.

To exclude the possibility that exchange from Pol III to Pol IV in Fig. 4 *C* and *E* is only observed as more rapid because of undersampling of Pol IV pauses in Fig. 4*A*, we simulated unbiased pause times expected from Fig. 4*A* using the fit constant of 16.8 s and the MATLAB exponential random number generator exprnd. One hundred independent datasets were generated, each with $n = 51$ to match the dataset in Fig. 4*A*; all produced pause time distributions that were slower than the exchange data from Pol III to Pol IV on undamaged DNA ($P < 10^{-5}$ for each vs. Fig. 4*C*) and at the N^2-furfuryl-dG lesion ($P < 0.01$ for each vs. Fig. 4*E*).

As expected, a similar analysis simulating unbiased data from pause times for Pol IV in experiments with the single-cleft clamp, β^+/β^C (Fig. S2*G*, $\tau = 17.9$ s, $n = 165$), produced pause distributions slower than exchange data from Pol III to Pol IV ($P < 10^{-8}$ for each vs. Fig. 4*C* and $P < 10^{-3}$ for each vs. Fig. 4*E*); therefore, the equally valid comparison of exchange data with Pol IV

pauses with β^{+}/β^{C} does not affect our conclusion that Pol III and Pol IV simultaneously bind β and rapidly exchange.

Because pauses between rapid Pol III events are not similarly undersampled, this analysis was not required for Fig. 4 *B*, *D*, and *F*, and the statistical comparisons reported were from the data displayed in Fig. 4.

Bulk Primer Extension Reactions. Running start bulk primer extension reactions (Fig. S5*A*) were performed using the template 5′-CTA CCT **X**TG GAC GGC TGC GA-3′ (**X** = N^2-furfuryl-dG or the dG control) annealed with the 5′-^{32}P-phosphorylated primer 5′-TCG CAG CCG T-3′ in replication buffer with either 50 nM Pol III or Pol IV; 30-μL reactions containing the primer template (20 nM final) were initiated by adding dNTPs (250 μM) and incubating at 37 °C. At the indicated times, 3 μL each reaction was added to 10 μL stop buffer (50 mM Tris·HCl, pH 7.5, 25 mM EDTA, 0.5% SDS). The control reaction lacking dNTPs was stopped after 15 min. Samples were separated on a 12% (wt/vol) urea-PAGE gel, and the dried gel was exposed to a phosphor screen and imaged with a Personal Molecular Imager (BioRad).

Modeling of the Structure of a Pol III–Pol IV-β Complex. Fig. S9, prepared in PyMOL (Schrödinger), was based on a previously published model of the closed Pol III αεθ complex bound to DNA and β derived from structures of individual subunits and constraints from NMR, small-angle X-ray scattering, and cross-linking (11). The structure of Pol IV (Protein Data Bank ID code 4IR9) (12) was docked onto the rim site of β using the cocrystal structure of the Pol IV little finger domain bound to β (Protein Data Bank ID code 1UNN) (13). Docking resulted in a minor clash with the fingers domain of the Pol III α-subunit at residue 95 of Pol IV but no other clashes. The clamp-binding motif of Pol IV is disordered in the Pol IV structure (12) but would be positioned to replace the α–clamp-binding motif on a transient release from the cleft.

1. Beuning PJ, Simon SM, Godoy VG, Jarosz DF, Walker GC (2006) Characterization of *Escherichia coli* translesion synthesis polymerases and their accessory factors. *Methods Enzymol* 408:318–340.
2. Maul RW, Ponticelli SK, Duzen JM, Sutton MD (2007) Differential binding of *Escherichia coli* DNA polymerases to the β-sliding clamp. *Mol Microbiol* 65(3):811–827.
3. Wijffels G, et al. (2004) Inhibition of protein interactions with the β_2 sliding clamp of *Escherichia coli* DNA polymerase III by peptides from β_2-binding proteins. *Biochemistry* 43(19):5661–5671.
4. Hamdan S, et al. (2002) Hydrolysis of the 5′-p-nitrophenyl ester of TMP by the proofreading exonuclease (ε) subunit of *Escherichia coli* DNA polymerase III. *Biochemistry* 41(16):5266–5275.
5. Oakley AJ, et al. (2003) Flexibility revealed by the 1.85 Å crystal structure of the β sliding-clamp subunit of *Escherichia coli* DNA polymerase III. *Acta Crystallogr D* 59(Pt 7):1192–1199.
6. Scouten Ponticelli SK, Duzen JM, Sutton MD (2009) Contributions of the individual hydrophobic clefts of the *Escherichia coli* β sliding clamp to clamp loading, DNA replication and clamp recycling. *Nucleic Acids Res* 37(9):2796–2809.
7. Tanner NA, et al. (2008) Single-molecule studies of fork dynamics in *Escherichia coli* DNA replication. *Nat Struct Mol Biol* 15(2):170–176.
8. Jarosz DF, Godoy VG, Delaney JC, Essigmann JM, Walker GC (2006) A single amino acid governs enhanced activity of DinB DNA polymerases on damaged templates. *Nature* 439(7073):225–228.
9. Delaney JC, Essigmann JM (2006) Assays for determining lesion bypass efficiency and mutagenicity of site-specific DNA lesions *in vivo*. *Methods Enzymol* 408:1–15.
10. Tanner NA, van Oijen AM (2010) Visualizing DNA replication at the single-molecule level. *Methods Enzymol* 475:259–278.
11. Ozawa K, et al. (2013) Proofreading exonuclease on a tether: The complex between the E. coli DNA polymerase III subunits α, epsilon, θ and β reveals a highly flexible arrangement of the proofreading domain. *Nucleic Acids Res* 41(10):5354–5367.
12. Sharma A, Kottur J, Narayanan N, Nair DT (2013) A strategically located serine residue is critical for the mutator activity of DNA polymerase IV from *Escherichia coli*. *Nucleic Acids Res* 41(9):5104–5114.
13. Bunting KA, Roe SM, Pearl LH (2003) Structural basis for recruitment of translesion DNA polymerase Pol IV/DinB to the β-clamp. *EMBO J* 22(21):5883–5892.

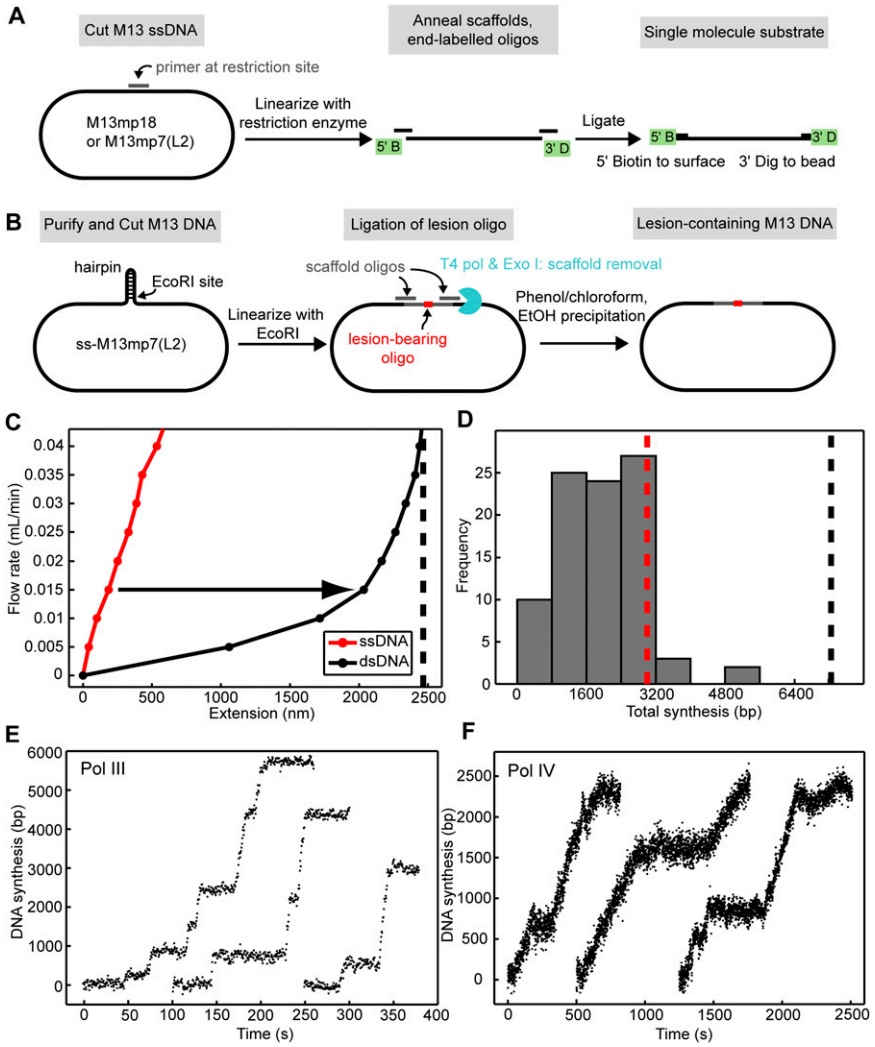

Fig. S1. A single-molecule primer extension assay. (*A*) A schematic of the construction of single-molecule substrates from M13 phage genomes: the circular ssDNA is linearized with a restriction enzyme and end-labeled using scaffold-mediated ligation. (*B*) A schematic of the generation of ssDNA containing a site-specific lesion: an internal hairpin is cleaved with EcoRI, and a chemically synthesized, lesion-containing oligonucleotide is ligated with scaffolds to recircularize the molecule. Excess primers and scaffolds are removed using T4 DNA polymerase and exonuclease I. (*C*) The differential extensions of ssDNA and dsDNA at increasing flow rates. dsDNA was generated from the single-molecule substrate stock using ϕ29 DNA polymerase (New England Biolabs). The conversion factor (3.9 bp nm^{-1}) used to calculate DNA synthesis from bead displacement was determined by dividing the total substrate length, 7,249 bp, by the difference in the extension of dsDNA and ssDNA at 0.015 mL min^{-1} (1,848 nm). (*D*) Annealing a 3′-dideoxy–terminated oligonucleotide onto the ssDNA substrate at the +3,000-bp position blocks synthesis by T7 DNA polymerase exo^{-} in 95% of trajectories (n = 91), confirming the conversion factor. The predicted location of the oligonucleotide block is marked with a dotted red line, and the full length of the substrate is marked with a dotted black line. Example trajectories for (*E*) Pol III (5 nM) and (*F*) Pol IV (30 nM). Initial time points are shifted for clarity; note different scales of axes.

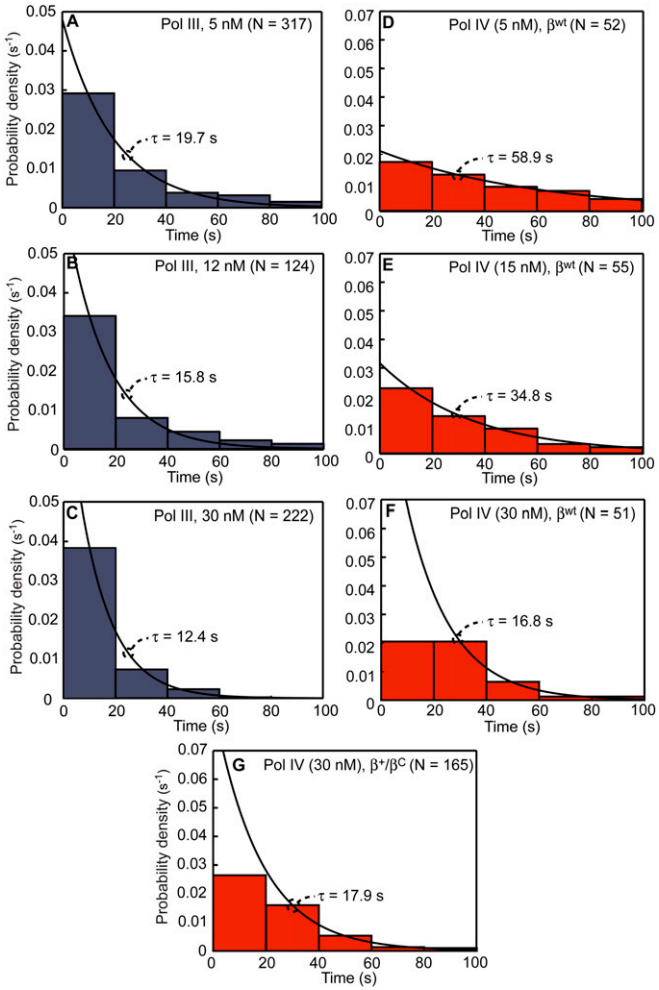

Fig. S2. Effects of polymerase concentration and the number of clefts on pausing. Pauses between polymerase synthesis events in single-molecule trajectories are exponentially distributed, suggesting a single rate-limiting step, and inversely related with concentration; increasing Pol III from (*A*) 5 to (*B*) 12 and (*C*) 30 nM or Pol IV from (*D*) 5 to (*E*) 15 and (*F*) 30 nM reduces these pause times. These data demonstrate that pauses observed during synthesis by Pol III or Pol IV alone represent dissociation of a polymerase followed by the diffusion-limited recruitment of another from solution. Association times (pauses) of Pol III are shorter because of a greater K_a for clamp binding measured in surface plasmon resonance experiments (1). Pauses observed in 30 nM Pol IV experiments with (*G*) the single-cleft clamp, β^{+}/β^{C}, are not significantly different from pauses observed in experiments with the WT clamp, β^{WT}. Observed pauses are, therefore, not caused by switching between two Pol IV molecules potentially bound to the same β dimer; τ represents the exponential constant for fits to pause distributions. The first bins of *D*–*G* are undersampled because of limits on the experimental resolution and therefore, were not used for fits.

1. Heltzel JM, Maul RW, Scouten Ponticelli SK, Sutton MD (2009) A model for DNA polymerase switching involving a single cleft and the rim of the sliding clamp. *Proc Natl Acad Sci USA* 106(31):12664–12669.

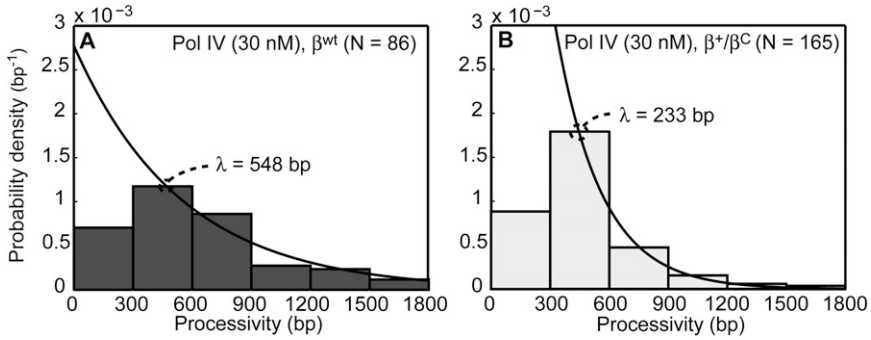

Fig. S3. Effect of the number of clefts available on Pol IV processivity. The observed processivity of Pol IV is greater in experiments with (*A*) β^{WT} than with (*B*) β^{+}/β^{C} ($P < 10^{-3}$), supporting structural data that two Pol IV molecules can bind a single β (1)—the apparent processivity is artificially increased by rapid, unresolvable switches between two polymerases bound to the clamp; λ represents the exponential constant for fits to processivity distributions. The first bins are undersampled because of limits on the experimental resolution and therefore, were not used for fits.

1. Bunting KA, Roe SM, Pearl LH (2003) Structural basis for recruitment of translesion DNA polymerase Pol IV/DinB to the β-clamp. *EMBO J* 22(21):5883–5892.

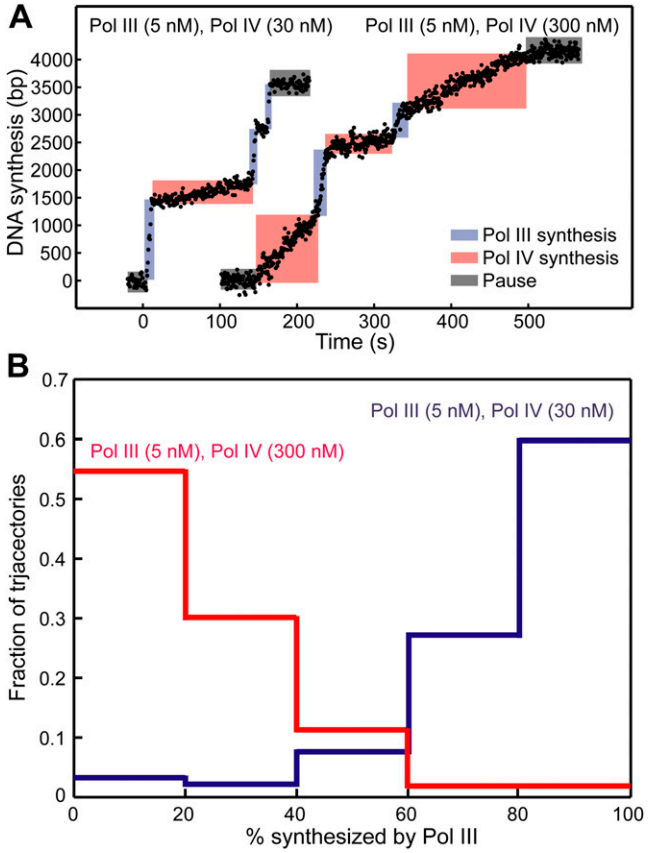

Fig. S4. Effects of increasing concentrations of Pol IV on competition with Pol III. (*A*) Example trajectories at a low and high ratio of Pol IV to Pol III with assignments. At high concentrations of Pol IV, individual pauses are no longer observable. (*B*) Distributions for the percent of synthesis completed by Pol III in individual trajectories in the presence of low (30 nM Pol IV, average of 78% Pol III synthesis; $n = 92$ trajectories) and high (300 nM Pol IV, 22% Pol III synthesis; $n = 53$) levels of Pol IV.

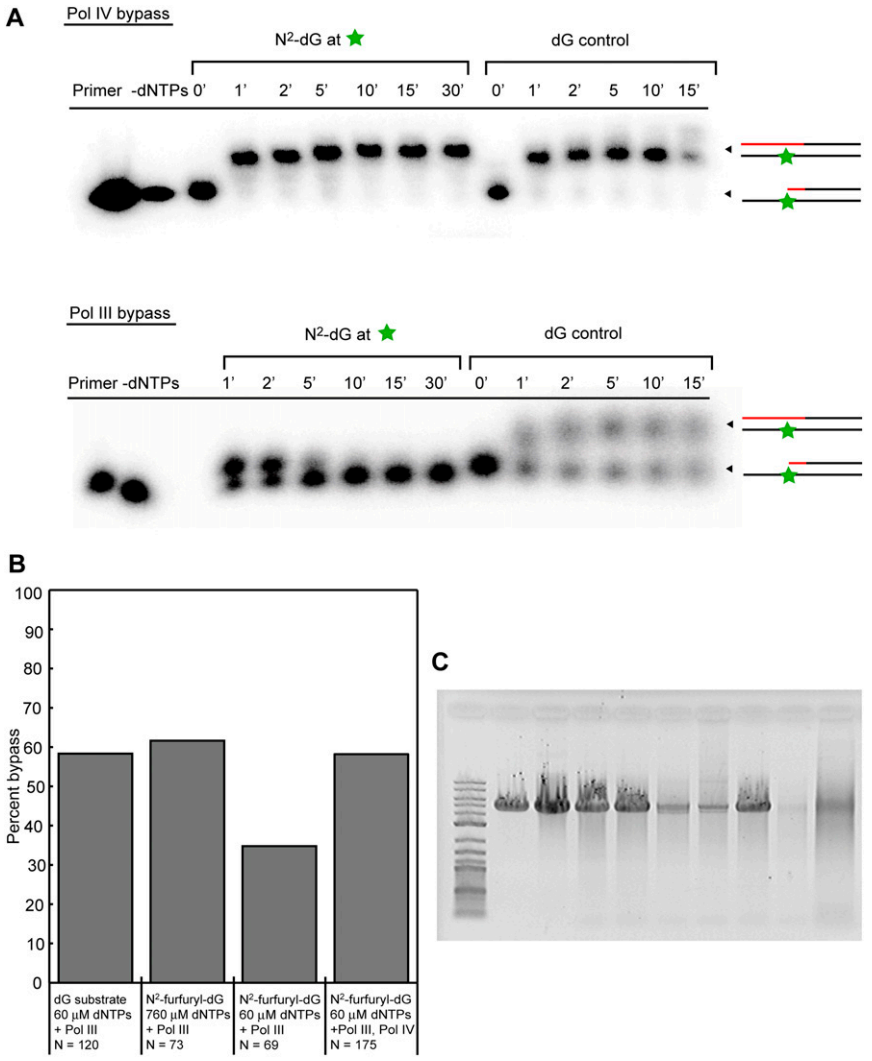

Fig. S5. Distributive and processive synthesis on templates containing a site-specific N^2-furfuryl-dG lesion. (*A*) A time course for distributive synthesis (in the absence of β) by Pol III or Pol IV on an oligonucleotide template with an N^2-furfuryl-dG (left side) or control dG (right side) base at the +3 position from the primer terminus. The lesion is a strong block for Pol III but rapidly bypassed by Pol IV. Arrows denote the location of the labeled 10-mer primer and the fully extended 20-mer product. Degradation of the primer by Pol III for the −dNTP control and on the lesion template is incomplete because of the short primer and the large footprint of the Pol III core. (*B*) The percentage of trajectories that bypasses the lesion site in single-molecule experiments. Bypass is defined as synthesis past the site plus 3σ of the noise (3,350 bp). Different conditions include lesion and control substrates, low and high dNTP concentrations, and with or without Pol IV. (*C*) Successive steps of preparation of lesion-containing M13 ssDNA; each lane of the agarose gel contains 700 ng DNA or the equivalent amount of the reaction unless otherwise specified. Lanes are numbered 1–10 from the left side: lane 1, 2-log ladder (5 μL; New England Biolabs); lane 2, M13mp18 ssDNA (New England Biolabs); lane 3, purified M13mp7L2 ssDNA; lane 4, after EcoRI digestion and subsequent purification; lane 5, after scaffold-mediated ligation with lesion-containing insert; lane 6, after treatment with T4 DNA polymerase and exonuclease I; lane 7, purified N^2-furfuryl-dG M13mp7L2. Treatment of mock-ligated (using scaffolds but no insert) substrate shows that digestion of the hairpin is nearly complete: lane 8, M13mp7L2 after the mock ligation; lane 9, after treatment with T4 polymerase and exonuclease I; lane 10, the same but loading 10 times the amount as lane 9.

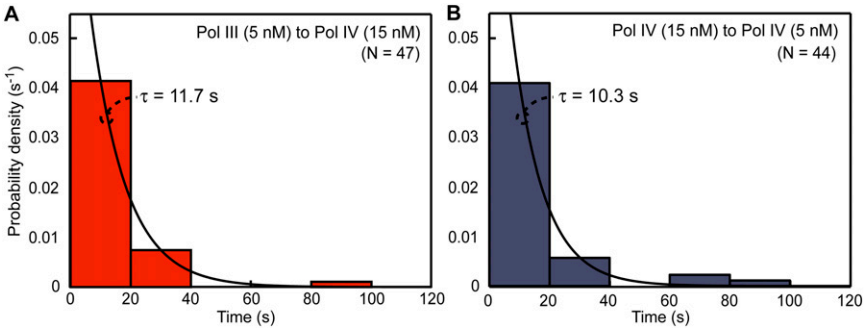

Fig. S6. Reducing the Pol IV concentration from 30 to 15 nM results in a timescale of exchange with Pol III statistically indistinguishable from Fig. 4*C*, despite the same dilution increasing the association time in experiments with Pol IV alone (Fig. S2 *E* and *F*). Exchange from (*A*) Pol III (5 nM) to Pol IV (15 nM) is more rapid than pauses in experiments with 15 nM Pol IV ($P < 10^{-5}$ vs. Fig. S2*E*); exchange from (*B*) Pol IV to Pol III remains rapid ($P < 10^{-7}$ vs. Fig. 4*A*).

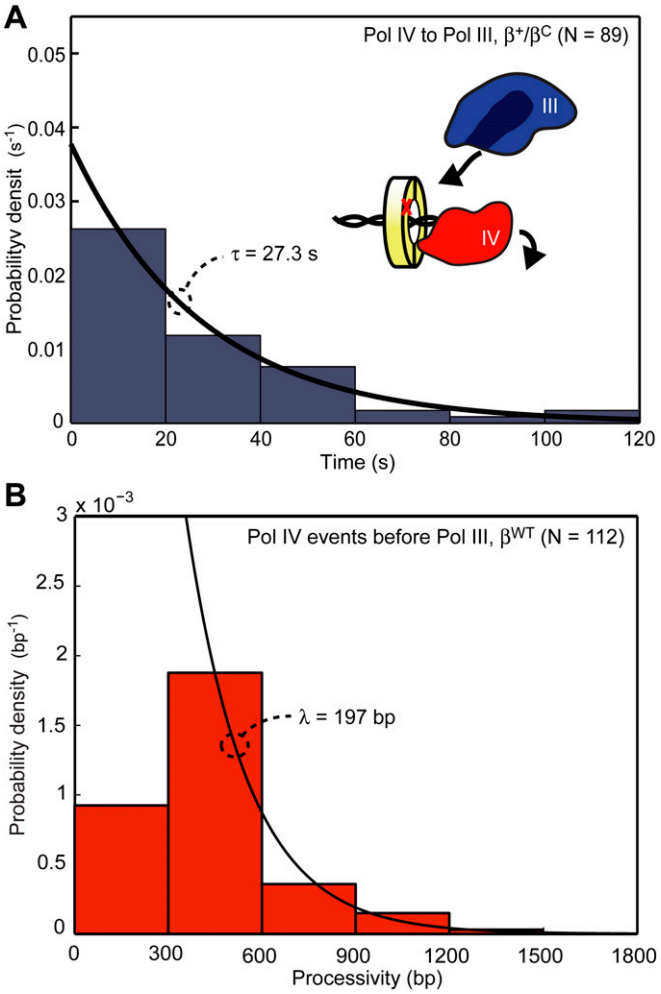

Fig. S7. Stoichiometry of Pol III and Pol IV on the clamp during rapid exchange. (*A*) Exchange from Pol IV (5 nM) to Pol III (30 nM) is diffusion-limited (*NS* vs. Fig. 4*B* and $P < 10^{-3}$ vs. Fig. 4*D*) in experiments with the single-cleft clamp, β^{+}/β^{C}, further showing that Pol III requires access to the free cleft to bind the clamp during Pol IV synthesis. (*B*) The processivity of Pol IV events preceding exchange to Pol III is less than the processivity of Pol IV alone (30 nM) with β ($P < 10^{-3}$ vs. Fig. S3*A*) and not significantly different from Pol IV with β^{+}/β^{C} (Fig. S3*B*), showing that a single Pol IV, at low concentrations, binds the clamp during exchange with Pol III.

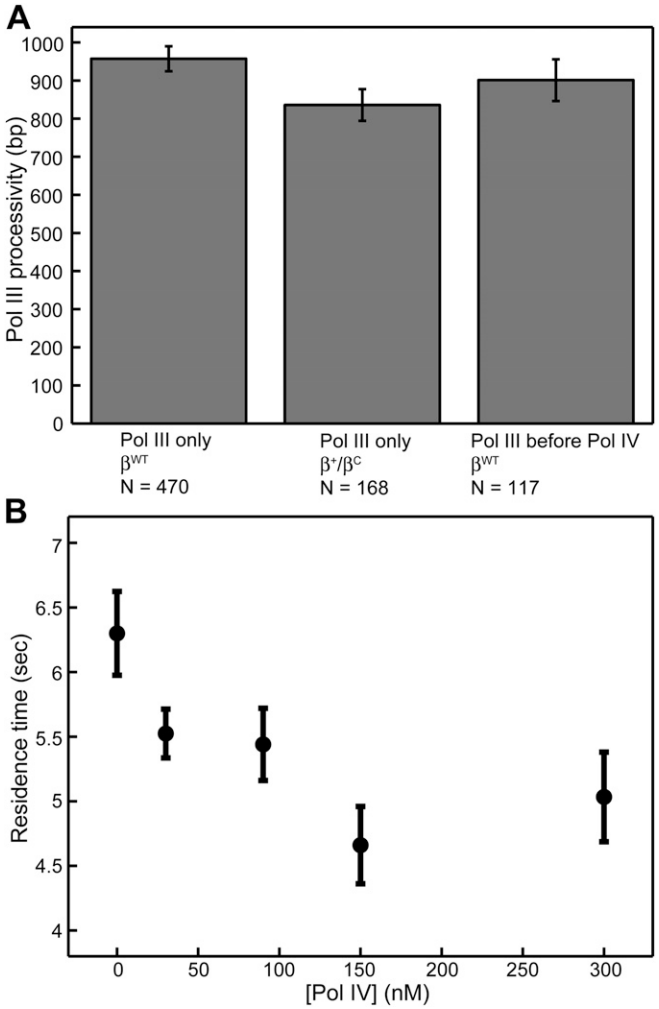

Fig. S8. Effects of Pol IV at low and high concentrations on Pol III stability. (*A*) Pol III processivity is modestly reduced by the absence of the ε–β contact and similarly reduced by the presence of Pol IV on the clamp, suggesting that Pol IV can compete with ε for a cleft. The average Pol III processivity in the following experiments (left to right): Pol III only (5 nM) in experiments with the WT clamp, β^{WT}; Pol III only (5 nM) with the single-cleft clamp, β^{+}/β^{C}, which eliminates binding by the weaker ε exonuclease subunit clamp-binding motif; and Pol III (5 nM) events that precede Pol IV (30 nM) events with the WT cleft. A similar reduction in Pol III processivity was previously observed in single-molecule leading strand experiments when the ε clamp-binding motif was weakened (1). (*B*) The average lifetime of Pol III on the clamp for individual synthesis events decreases with increasing concentrations of Pol IV. The lifetime for each event was determined by dividing the processivity by the rate.

1. Jergic S, et al. (2013) A direct proofreader-clamp interaction stabilizes the Pol III replicase in the polymerization mode. *EMBO J* 32(9):1322–1333.

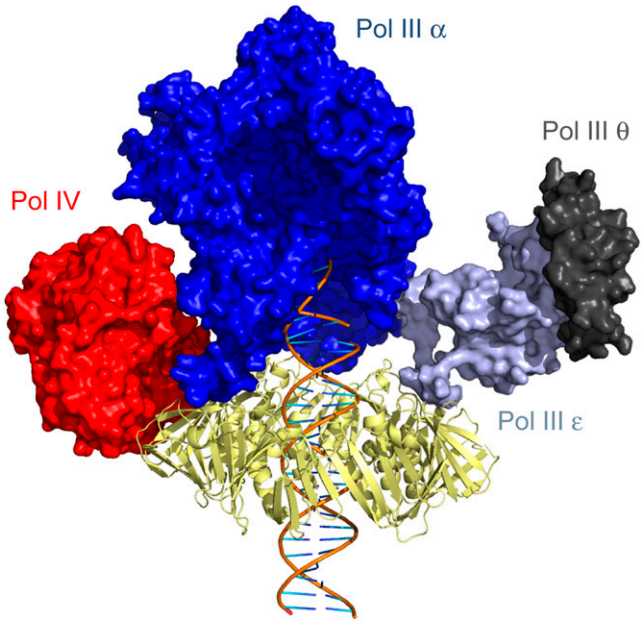

Fig. S9. Pol III and Pol IV bound to β (yellow), with Pol IV positioned at the rim site to capture the Pol III α clamp-binding motif during a transient release from its cleft. This model shows that concurrent binding of the two polymerases to the same protomer of β is consistent with structural data for Pol III and Pol IV and their clamp-binding modes. *SI Experimental Procedures* has details of model construction.

Table S1. Oligonucleotides (Integrated DNA Technologies) used to construct single-molecule substrates

Names	Sequences (5′ to 3′)
mp18-SalI	CTGCAGGTCGACTCTAGA
mp18-scaffold-1	GCGGGCAATATGTACCTCTAGAGGATCCCC
mp18-scaffold-2	ATGCCTGCAGGTCGAACTATGCGACTGGAC
mp7L2-AlwNI	AGCGCAGTCTCTGAATTTAC
mp7L2-scaffold-1	GCGGGCAATATGTACTCTCTGAATTTACCG
mp7L2-scaffold-2	GAATGGAAAGCGCAGACTATGCGACTGGAC
M13-3′-dig	GTACATATTGCCCGCAAAAAA-Dig
M13-5′-biotin	BioTEG-GTCCAGTCGCATAGT